ARTICLE

Effective Strain in Helical Rippled Carbon Nanotubes: A Unifying Concept for Understanding Electromechanical Response

Dong-Bo Zhang[†] and Traian Dumitrică[†,‡,*]

[†]Department of Chemical Engineering and Materials Science, University of Minnesota, Minneapolis, Minnesota 55455, United States, and [‡]Department of Mechanical Engineering, University of Minnesota, Minneapolis, Minnesota 55455, United States

ABSTRACT Despite its importance, little is known about how complex deformation modes alter the intrinsic electronic states of carbon nanotubes. Here we consider the rippling deformation mode characterized by helicoidal furrows and ridges and elucidate that a new intralayer strain effect rather than the known bilayer coupling and $\sigma-\pi$ orbital mixing effects dominates its gapping. When an effective shear strain is used, it is possible to link both the electrical and the mechanical response of the complex rippled morphology to the known behavior of cylindrical tubes. In combination with objective molecular dynamics, this concept may be useful for understanding the electromechanical characteristics of large scale carbon nanotube assemblies and other individual nanoscale forms of carbon.

KEYWORDS: carbon nanotubes · electromechanical characteristics · nanoelectromechanical devices · molecular dynamics · elasticity · resilience

Due to their superior strength[1,2] and resilience, combined with a tunable-by-strain electronic structure, carbon nanotubes (CNTs) are actively researched for use in nanoelectromechanical devices.[3−8] The changes in the electronic and thermal properties of nanoscale materials caused by reversible deformation modes have been under constant scrutiny.[9−26] So far, microscopic modeling has played an important role in understanding the physics underlying the nanotube electromechanical properties observed in experiment. In one class of experiments[10,11] with metallic CNTs, it was found that small band-gaps (less than ~100 meV) open up in response to lateral mechanical squeezing. Relying on density functional theory calculations, this behavior could be clearly attributed to the bilayer-coupling that arises between the two sides of the flattened tube.[12] Tight binding (TB) molecular dynamics (MD) demonstrated that another known effect, the $\sigma-\pi$ orbital mixing due to the creation of inhomogenous curvature, is secondary and could become important under very severe squeezing.[13]

The electromechanical consequences of the long known helical rippling that develops during similar mechanical manipulation, that is, the locked twist state of a collapsed CNT,[27,28] are not yet understood. Many effects (or combinations) could be important and unfortunatley standard electronic structure calculations become prohibitive for such complicated morphologies. It is suggested that the observed changes in the electronic states[28] originate in the same bilayer coupling and $\sigma-\pi$ orbital mixing effects. CNTs under torsion are prone to similar rippling deformations characterized topologically by extended helicoidal ridges and furrows of positive and negative curvature, respectively. In another class of experiments[4,6,17,20] single-walled (SW) and multiwall (MW) CNTs are employed as torsional springs. Notably, these nanotube-pedal experiments make available both the torque experienced by a CNT and its electrical conductance response to continuous twisting.

From a mechanical viewpoint, rolling of the isotropically elastic graphene into a cylindrical SWCNT is practically linear,[29] that is, at moderate diameters it does not couple with other deformations, such as twisting. For example, microscopic calculations found an intrinsic twist of only 0.04 deg/nm[30] in a (14,6) SWCNT, much smaller than the 0.87 deg/nm twist stored by its (14,6) MoS_2 NT counterpart.[31] Thus, the elastic[32] and electronic[33,34] intrinsic properties of SWCNT can be readily linked to those of flat graphene. For example, the electronic bands of a SWCNT of radius R are equispaced $1/R$ sub-bands in graphene's band structure, labeled[34] by the angular quantum number l.

*Address correspondence to td@me.umn.edu.

Received for review August 9, 2010 and accepted October 4, 2010.

Published online October 14, 2010. 10.1021/nn1019658

For a (n, n) SWCNT, $l = 0,..., n - 1$ and k_F, the Fermi momentum of graphene, is located on the $l = 0$ sub-band. Notably, the changes imposed on the electronic states by a homogeneous deformation can be still derived from the flat graphene picture. A CNT's response to an atomic scale torsional deformation is described by the Yang and Han (YH) nonperturbative model,[9] formulated in terms of π-orbitals. The key features are as follows: When applying a torsional rate Γ, the wall of an ideal SWCNT experiences a homogeneous shear strain ΓR. The sub-bands remain invariant under torsion. In a (n, n) SWCNT torsion shifts the location of k_F in the circumferential direction by $\Delta k_F = \Gamma R/d_{C-C}$, where d_{C-C} is the equilibrium C−C bond length. Due to the linearity of the dispersion relation near k_F, the band gap variation of a SWCNT is proportional to Δk_F. When $\Delta k_F = 1/R$, k_F reaches the $l = 1$ sub-band, the band gap of the twisted tube closes. The band gap is maximum at the midpoint between these two sub-bands. This predicted behavior was recently obtained[35] by direct simulations with a generalization of periodic MD termed objective MD.[36,37]

Here we develop an effective shear strain theory for the electromechanical response of rippled CNTs and show that an intralayer effect, not considered before, dominates the gapping of metallic tubes. We first focus on isolated SWCNTs and uncover the dominant role played by the inhomogenous helical strain present in the rippled wall. A developed π-orbital TB perturbative treatment captures the bilayer-coupling effect and defines an effective shear strain under which the intrawall band gap variations follow the ideal YH recurrent behavior. These predictions are confirmed by objective MD calculations performed on a four-orbital helical-symmetry adapted basis.[37−41] Next, we simulate the consequences of the gradual presence of interior walls and demonstrate that the effective strain has a clear mechanical interpretation. Finally, we discuss the experimental implications of our findings. We suggest that some caution should be taken when using the YH model to interpret the conductivity measurements carried out in CNT-pedal devices especially when SWCNTs and MWCNTs with large diameters and a small number of walls are employed.

RESULTS AND DISCUSSION

Our initial objective MD simulations considered specifically a (30,30) SWCNT because such a large-radius tube is very susceptible to collapse[42] and rippling.[35] Upon a smooth variation of Γ, the tube exhibits large hysteresis in twisting−untwisting cycles, with stable and metastable rippling states. When complete untwisting occurs, this SWCNT is locked in a purely collapsed state[42] for which gapping is well understood.[12] Figure 1a suggests that rippling should affect the electronic states since a large portion of the van der Waals contact stacks in a Bernal lattice pattern.

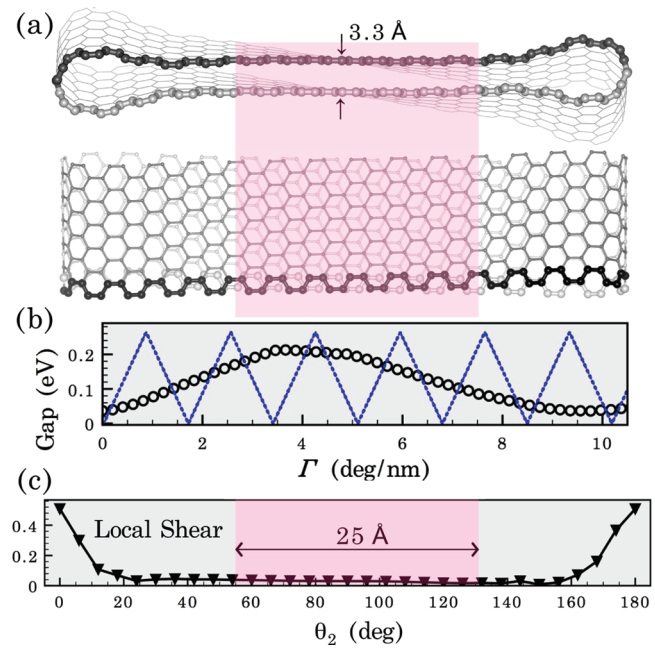

Figure 1. (a) Cross section (top) and side (bottom) views of a two-lobe rippled (30,30) SWCNT under 10.7 deg/nm twist, as computed with objective MD. Neighboring objective motifs are generated by translating and rotating around the SWCNT axis the 4*n* atoms shown with balls. (b) Band-gap *vs* the applied twist rate for the rippled state (circles). The ideal YH behavior (dotted) is shown for a comparison. (c) Circumferential distribution of the averaged shear strain on atom *A*. Shading indicates the region at the furrows stacked in a Bernal pattern.

We first attempt to rationalize the bilayer-coupling effect in the framework of simple π-orbital TB and modeled it with degenerate perturbation theory with respect to the intrinsic states of the cylindrical untwisted SWCNT. Only two quantities are essential: t, the intralayer hopping between the A and B sublattices, and γ, the effective interlayer coupling between the AA sites. A (n,n) SWCNT is constructed from a two-atom AB cell under repeated N helical (typically ∞) and n azimuthal operations,[32,34] indexed by ζ_1 and ζ_2, respectively. The electronic bands $E_{l\kappa}$ under an arbitrary Γ are labeled also by the helical quantum number $-\pi \leq \kappa < \pi$. Their eigenstates are represented in terms of two symmetry-adapted Bloch sums[35]

$$|j, l\kappa\rangle = \frac{1}{\sqrt{nN}} \sum_{\zeta_1=0}^{N-1} e^{i\kappa\zeta_1}(|j, \zeta_1\rangle + e^{il\pi}|j, \zeta_1\rangle'), \; j = A, B \tag{1}$$

Here $|j, \zeta_1\rangle$ and $|j, \zeta_1\rangle'$ are partial sums $\Sigma_{\zeta_2} e^{il\theta_2\zeta_2}|j, \zeta_1\zeta_2\rangle$, with angular index ζ_2 limited over the upper (dark balls, Figure 1a) and lower circumferential half (light gray balls, Figure 1a), respectively. $|j, \zeta_1\zeta_2\rangle$ is the symmetry-adapted π-orbital on the atom j of the ζ_1 and ζ_2 site, and $\theta_2 = 2\pi/n$. At the κ points corresponding to the metallic state, the interaction of the furrows couples strongly the valence and conduction bands with the same l *via* the proposed Hamiltonian

$$H_l = \begin{pmatrix} \gamma \cos \pi l & \sum_\eta t f_\eta(l,\kappa) \\ \sum_\eta t f_\eta^*(l,\kappa) & 0 \end{pmatrix} \quad (2)$$

Index η runs over the three intralayer nearest-neighbor atoms and $f_\eta(l, \kappa)$ is the difference in Bloch factors. The weaker coupling between the other pairs of sublattices can be included in (eq 2) by simple modifications. The bilayer-coupling yields the quadratic dispersion

$$\left(E_{l\kappa} - \frac{\gamma}{2}\cos \pi l\right)^2 = \left(\frac{\gamma}{2}\cos \pi l\right)^2 + \left|\sum_\eta t f_\eta(l,\kappa)\right|^2 \quad (3)$$

The fundamental band gap is given by the effective coupling strength γ, which depends on the separation distance between the faces and the fraction of the tube in close contact.[43] The rigid $\gamma/2$ shift in energy (left side of the equality) only moves the bands with even (odd) l up (down).

Figure 1b indicates that the band gap given by the objective MD simulations exhibits a recurrent variation with Γ that is very different from the ideal YH one. The band gap γ of ~40 meV for the purely collapsed (30,30) SWCNT ($\Gamma = 0$ deg/nm) is much smaller than, for example, the ~200 meV gap calculated for the rippled state at $\Gamma = 4$ deg/nm. By examining the computed rippled morphologies, we determined that the fraction of the tube stacked in the Bernal patterns is maintained throughout the twisting process. Furthermore, unlike in the case of laterally applied squeezing,[12,11] the twisted tubes are free to relax in the radial direction. Hence, the separation between furrows is practically pinned at the ~3.3 Å van der Waals equilibrium distance even at the highest twist rate considered, Figure 1a. Thus, the bilayer-coupling effect alone cannot account for the obtained bang gap variations with Γ. What else, besides the bilayer-coupling of the furrows, takes place in the course of twisting?

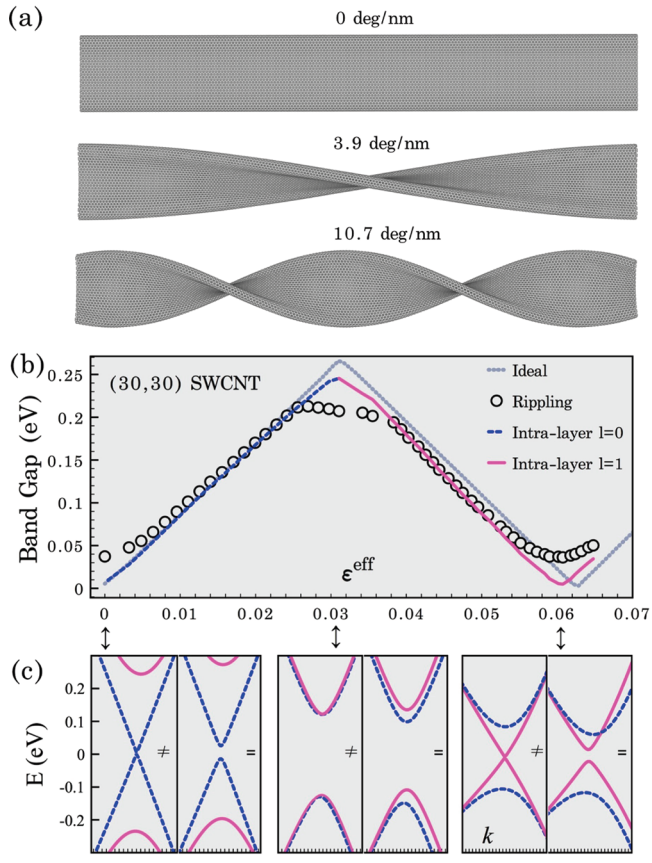

Figure 2. (a) Two-lobe rippling (side view) in a (30,30) SWCNT under twist. The shown length is 44 nm. (b) Band-gap for a (30,30) SWCNT, ideal (dotted) and two-lobe rippling (circles), *vs* the effective shear strain. The intralayer contribution is shown for a comparison. (c) Closeups of the two bands around the Fermi level (set to zero) for the two-lobe rippling mode, without (≠) and with (=) bilayer-coupling, at three ε^{eff} (Γ) values, 0 (0 deg/nm) left, 0.03 (3.9 deg/nm) center, and 0.06 (10.7 deg/nm) right. The dashed (continuous) lines are bands with $l = 0$ ($l = 1$).

Rippling creates an inhomogeneous shear strain distribution, an effect that is not present in the collapsed armchair CNTs. Thus, we considered another effect: gapping by shear strain. Figure 1c confirms the presence of local shear strain in typical two-lobe rippling. Around the circumference, one can distinguish a low-strain nearly homogeneous region located at the furrows and a narrow high-strain region at the ridges. Such distribution of strain suggests a perturbative picture in which most of the SWCNT is under the influence of the averaged strain at the furrows ε^f, and the unperturbed band gap follows the YH behavior with a period d_{C-C}/R. We use the framework provided by the simple π-orbital TB and the Bloch sum basis (1) to account for the perturbation introduced by the averaged strain at the ridges ε^r. Ignoring the orbital rotation effect, the outcome of shear[9] is captured in the off-diagonal elements of (eq 2) *via* the dependence of the hopping parameter t_η on the bond length under shear d_η, as $t_\eta \sim t(d_{C-C}/d_\eta)^2$. If the perturbation acts alone, the eigenspectrum writes

$$E_{l\kappa}^2 = \left|\sum_\eta (t_\eta(\varepsilon^f) + n_r[t_\eta(\varepsilon^r) - t_\eta(\varepsilon^f)])f_\eta(l,\kappa)\right|^2 = \left|\sum_\eta t_\eta(\varepsilon^{eff}) f_\eta(l,\kappa)\right|^2 \quad (4)$$

where n_r is the fraction of A atoms at the ridges and $\varepsilon^{eff} = \varepsilon^f + n_r(\varepsilon^r - \varepsilon^f)$. Thus, we predicted that the intralayer band gap variations would still follow the YH behavior but under a redefined average strain ε^{eff}. On the basis of the analogy with the popular effective mass of electrons concept, we interpret ε^{eff} as the actual effective strain felt by the electronic system. The ε^{eff} effect could dominate gapping, as twist creates a band gap typically much larger than the bilayer-coupling one.

To probe the above prediction, we have reconsidered the band gap data, containing both the bilayer coupling and intralayer shear contributions, in the ε^{eff} context. The latter quantity, measured here from the

rippled SWCNT atomic positions[44] at each twist level, exhibits a nearly linear dependence on Γ and equals ΓR for the ideal SWCNT. Some representative snapshots of uniformly twisted morphologies are shown in Figure 2a. Surprisingly, Figure 2b indicates that the YH dependence is now followed very well, which clearly demonstrates that the electronic response is dominated by the intralayer contribution.

In comparison with the intrawall strain effect, the bilayer-coupling one remains secondary. It contributes mainly at the cusp points of the YH variations: As carefully detailed in the band structures of Figure 2b, when the intralayer band gap vanishes, the coupling of the $l = 0$, Figure 2c, left, and $l = 1$ bands, Figure 2c, right, creates a direct band gap, a behavior captured by (eq 3). In the strain region around the central maximum, the intralayer valence-conduction gaps of the $l = 0$ and $l = 1$ bands become comparable in size and are exactly equal at the cusp, Figure 2c, middle. The preferential $\gamma/2$ shift predicted by eq 3 and irrelevant at other strain levels now becomes important. By shifting the $l = 0$ ($l = 1$) bands downward (upward), the bilayer coupling creates a lower, indirect band gap. Note that in Figure 2c, left and right, gap opening is solely due to the bilayer coupling. The identity in band gap values for these purely collapsed and severely twisted states demonstrates once more that the coupling strength γ does not change throughout the twisting process. Finally, we conclude that because all the important features in Figure 2 can be explained in terms of ε^{eff} and bilayer-coupling *via* eqs 3 and 4, respectively, the alternative $\sigma-\pi$ mixing effect practically has no effect on the band structure around the Fermi point.

Further objective MD simulations indicated that MWCNTs also exhibit stable two-lobe rippling,[35] Figure 3a, and practically lack hysteresis effect in the twisting−untwisting cycle. The critical torsional strain marking the onset of rippling increases significantly as the core space of the (30, 30) SWCNT is filled with concentric tubes, Figure 3b. It is interesting to examine the effect of the inner walls on the ε^{eff} in the outermost wall, Figure 3c. At a given Γ, the double-walled CNT has the lowest ε^{eff}. Rippling fades with the further addition of inner walls as the distinction between ε^{eff} and ΓR gradually washes out. In all cases, ε^{eff} keeps a nearly linear dependence on Γ.

So far we have discussed ε^{eff}, derived earlier from the simple π-orbital model, only in the electrical domain. Notably, we find that the concept is retained in the mechanical domain, when σ bonding is significant. From the objective MD data, the rippling-induced changes in the elastic response of the outer wall can be obtained by studying the strain energy *vs* Γ relation. For all the tested MWCNTs, we find that the rippled outermost wall exhibits a nearly linear elastic response with a reduced torsional constant when compared with the ideal state. This behavior can be clearly observed in the

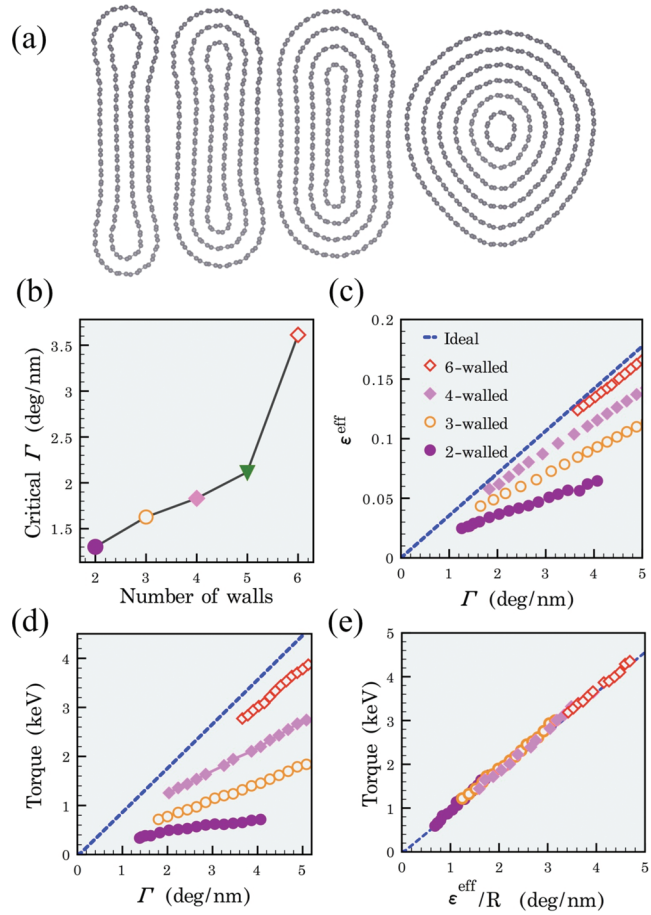

Figure 3. Two-lobe rippling (cross-sectional view) in a MWCNT family with (30,30) tube as the outermost wall, as obtained by objective MD simulations. (b) Critical strain for rippling *vs* the number of walls. (c) Effective strain in the outermost wall *vs* applied twist rate. Torque in the outer wall (d) *vs* twist rate and (e) *vs* effective strain. Dashed line is the idealized case.

torque (energy derivative with Γ) *vs* Γ plots of Figure 3d, where the slope represents the torsional constant. Comparing Figure 3c and d, one notes a striking correlation in how ε^{eff} and torque depend parametrically on the number of inner walls. It suggests that the apparent decrease in the torsional constant originates in the lower-than-ideal effective strain felt by the CNT wall. Indeed, when plotting the torque *vs* ε^{eff} scaled by the CNT radius, Figure 3e, data collapses onto the ideal behavior. Physically, it means that rippling lowers the strain energy by lowering the strain felt by the CNT wall without affecting much the original sp^2 bonding of flat graphene.

The finding that the helical rippled MWCNTs store an effective shear strain brings a new perspective to the observed[28] electronic structure changes occurring in locked helical-rippled MWCNTs, having morphologies similar to the ones simulated in Figure 4a. As yet, only presuppositions based on bilayer-coupling and $\sigma-\pi$ orbital mixing have been formulated. Regarding the MWCNT-pedal experiments, recent work[20] elucidated that the measured conductance oscillations originate in the twist-induced band gap variations of the outermost wall. The following question is of central im-

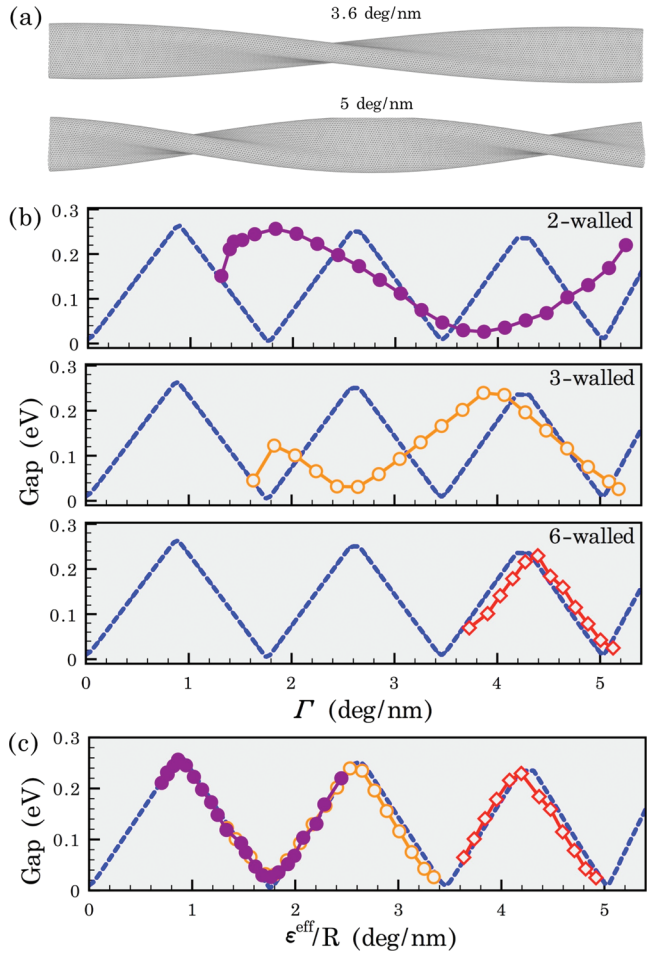

Figure 4. (a) Snapshots of a (30,30) outermost wall (side view) in a 3-walled MWCNT under two levels of twist. The shown length is 60 nm. Band-gap in the rippled (30,30) outermost wall of a 2-, 3-, and 6-walled MWCNT *vs* (b) the applied twist and (c) the effective strain. Dashed line is the idealized case.

portance: Is it possible to interpret these conductance oscillations with the ideal YH model? For an ideal armchair MWCNT of radius R, the YH oscillation period is d_{C-C}/R^2. However, as it can be seen in Figure 4b, the interlayer band gap modulations computed for the (30,30) outermost wall have various oscillation periods with Γ, depending on the number of inner walls. As in a previous work,[35] Figure 4b seems to suggest a negative answer except for the closed core MWCNT case, where $\varepsilon^{eff} \sim \Gamma R$. However, all band gap data collapses onto the ideal behavior when plotted against ε^{eff}, Figure 4c. Thus, in the ε^{eff} rescaling, the YH model can be applied with confidence to any CNT. The knowledge of ε^{eff} becomes particularly important for large diameter MWCNTs with a small number of walls. We envision that in a nanotube-pedal experiment, ε^{eff} can be also extracted from both the electrical and mechanical domains. When the assumption that ε^{eff} has simple linear dependence on γ is used, as obtained in Figure 3c, the applied twist rate could be easily rescaled such as the measured electrical conductivity and torque data collapses onto the ideal behavior, as obtained in Figure 4c and Figure 3e.

CONCLUSIONS

In conclusion, new findings often come by using new concepts and tools. Combining the effective shear strain with the objective MD, we elucidated the electronic response of complex rippled SWCNTs and MWCNTs and demonstrated that it can be linked to the known behavior of ideal cylindrical tube counterparts *via* a simple π-orbital TB formalism. This interesting manifestation of CNT's resilience can be further applied for studying other complex deformation modes, such as rippling of MWCNTs under bending.[45] Additionally, the presented methodology allows for examining tunability of other important physical properties, like electrical conductivity in twisted CNTs and calls for generalizing the standard translational-invariant formalisms to the helical symmetry and the objective structure concept.[46]

It is well documented that SWCNTs mainly of the (10,10)-type grow in bundles, forming a two-dimensional triangular lattice with a diameter of around 17 Å. The individual SWCNT in bundle can adopt a twisted form.[47] Atomistic simulations[48] of twisted bundles obtained helical rippling in the individual SWCNTs, similar with the ones studied here. Thus, the ε^{eff}-based theory introduced here for dealing with individual CNTs, might find use for studying large scale CNT assemblies. It is likely that the band gap modulation caused by the intrawall mechanism in the individual SWCNT dominates the known intertube coupling effect.[49]

The effective strain concept and objective MD can be applied for analyzing other nonideal nanoscale forms of carbon, such as graphene nanoribbons. For example, it is known that the reconstruction at the edges could force these ribbons to abandon their two-dimensional planarity and acquire an intrinsic twist.[50,51] This remarkably simple phenomenon could be used to develop stress-free helical graphene nanostructures with properties tunable by the amount of stored effective strain.

METHODS

Our microscopic simulations were performed with objective MD. A rigorous justification of this method and its tight-binding formulation are given in refs 36 and 37. In the current study, this technique brings the important ability to microscopically simulate the large scale helical rippled states of both SWCNTs and MWCNTs of armchair type by considering only the $4n$ atoms per wall located at positions $\mathbf{X}_i$ inside a primitive motif, Figure 1a. Specifically, a twisted CNT is described as an objective molecular structure,[36,46] with

$$\mathbf{X}_{i,\zeta} = \mathbf{R}^{\zeta}\mathbf{X}_i + \zeta\mathbf{T} \qquad (5)$$

Here, $\mathbf{X}_{i,\zeta}$ are the atomic locations inside the objective motif replica ζ, with $\zeta = 1, ..., N$. Rotational matrix $\mathbf{R}$ of angle θ and the axial

vector **T** characterize the discrete screw repetition rule applied to the atoms located inside a primitive motif. Eq 5 determines the objective MD of the twisted CNT. It represents the objective boundary conditions imposed over the 4*n* atoms, the analogous of the standard periodic boundary conditions of periodic MD. Note that although the group operations indicated by eq 5 are discrete, the simulated helical rippled morphologies are nicely smooth, as can be seen in Figures 1a, 2a, and 4a. Interestingly, the periodicity of a ripple is larger than |**T**|, is twist and number of walls dependent, Figures 2a, and 4a, and is the outcome of the objective MD simulation. The twist rate is defined as $\Gamma = \theta/|\mathbf{T}|$. If $\theta = 0$, the standard translational repetition rule is regained.

For a high fidelity modeling of the ripped states, accurate accounting of both covalent and long-range van der Waals forces is needed. The simplification in the number of atoms introduced by objective MD makes tractable quantum mechanical treatments of the chemical bonding. Here we used the nonorthogonal density functional theory based tight-binding[40,52] extended to account for the van der Waals interactions.[41] This microscopic description has proven to be accurate for carbon systems,[35,41] yet it still permits sufficiently long (2−5 ps) MD simulations on systems large enough (~200 atoms) to detect the most favorable rippling morphologies, Figures 1a and 3a. The torsional strain Γ was carefully applied by varying θ in small increments. Objective MD was used as an optimization tool, by carrying out a combination of low temperature MD with a 1 fs time step followed by conjugate-gradient energy minimizations. Between 5 (for MD) and 101 (for structural relaxation) helical κ numbers were used to converge the band energy. All of the presented data was obtained based on the optimized geometries at the different strain levels.

Acknowledgment. Work supported by NSF CAREER Grant No. CMMI-0747684, NSF Grant No. 1006706, and AFOSR Grant No. FA9550-09-1-0339. Computations were carried out at the Minnesota Supercomputing Institute.

REFERENCES AND NOTES

1. Dumitrică, T.; Belytschko, T.; Yakobson, B. I. Bond-Breaking Bifurcation States in Carbon Nanotube Fracture. *J. Chem. Phys.* **2003**, *118*, 9485–9488.
2. Dumitrică, T.; Hua, M.; Yakobson, B. I. Symmetry-, Time-, and Temperature-Dependent Strength of Carbon Nanotubes. *Proc. Natl. Acad. Sci. U.S.A.* **2006**, *103*, 6105–6109.
3. Rueckes, T.; Kim, K.; Joselevich, E.; Tseng, G. Y.; Cheung, C. L.; Lieber, C. M. Carbon Nanotube-Based Nonvolatile Random Access Memory for Molecular Computing. *Science* **2000**, *289*, 94–97.
4. Fennimore, A. M.; Yuzvinsky, T. D.; Han, W.-Q.; Fuhrer, M. S.; Cumings, J.; Zettl, A. Rotational Actuators Based on Carbon Nanotubes. *Nature* **2003**, *424*, 408–410.
5. Sazonova, V.; Yaish, Y.; Ustunel, H.; Roundy, D.; Arias, T. A.; McEuen, P. L. A Tunable Carbon Nanotube Electromechanical Oscillator. *Nature* **2004**, *431*, 284–287.
6. Mayer, J. C.; Paillet, M.; Roth, S. Single-Molecule Torsional Pendulum. *Science* **2005**, *309*, 1539–1541.
7. Ke, C.; Espinosa, H. D. In Situ Electron Microscopy Electromechanical Characterization of a Bistable NEMS Device. *Small* **2006**, *2*, 1484–1489.
8. Hall, A. R.; Falvo, M. R.; Superfine, R.; Washburn, S. Electromechanical Response of Single-Walled Carbon Nanotubes to Torsional Strain in a Self-Contained Device. *Nat. Nanotechnol.* **2007**, *2*, 413–416.
9. Yang, L.; Han, J. Electronic Structure of Deformed Carbon Nanotube. *Phys. Rev. Lett.* **2000**, *85*, 154–157.
10. Tombler, T. W.; Zhou, C. W.; Alexseyev, L.; Kong, J.; Dai, H. J.; Lei, L.; Jayanthi, C. S.; Tang, M. J.; Wu, S. Y. Reversible Electromechanical Characteristics of Carbon Nanotubes under Local-Probe Manipulation. *Nature* **2000**, *405*, 769–772.
11. Minot, E. D.; Yaish, Y.; Sazonova, V.; Park, J. Y.; Brink, M.; McEuen, P. L. Tuning Carbon Nanotube Band Gaps with Strain. *Phys. Rev. Lett.* **2003**, *90*, 156401-1–156401-4.
12. Lu, J.-Q.; Wu, J.; Duan, W.; Liu, F.; Zhu, B.-F.; Gu, B.-L. Metal-to-Semiconductor Transition in Squashed Armchair Carbon Nanotubes. *Phys. Rev. Lett.* **2003**, *90*, 156601-1–156601-4.
13. Mehrez, H.; Svizhenko, A.; Anantram, M. P.; Elstner, M.; Frauenheim, T. Analysis of Band-Gap Formation in Squashed Armchair Carbon Nanotubes. *Phys. Rev. B* **2005**, *71*, 155421-1–155421-7.
14. Maiti, A. Carbon Nanotubes: Bandgap Engineering with Strain. *Nat. Mater.* **2003**, *2*, 440–442.
15. Gómez-Navarro, C.; de Pablo, P. J.; Gomez-Herrero, J. Radial Electromechanical Properties of Carbon Nanotubes. *Adv. Mater.* **2004**, *16*, 549–552.
16. Semet, V.; Binh, V. T.; Guillot, D.; Teo, K. B. K.; Chhowalla, M.; Amaratunga, G. A. J.; Milne, W. I.; Legagneux, P.; Pribat, D. Reversible Electromechanical Characteristics of Individual Multiwall Carbon Nanotubes. *Appl. Phys. Lett.* **2005**, *87*, 223103-1–223103-3.
17. Cohen-Karni, T.; Segev, L.; Srur-Lavi, O.; Cohen, S. R.; Joselevich, E. Torsional Electromechanical Quantum Oscillations in Carbon Nanotubes. *Nat. Nanotechnol.* **2006**, *1*, 36–41.
18. Stampfer, C.; Jungen, A.; Linderman, R.; Obergfell, D.; Roth, S.; Hierold, C. Nano-Electromechanical Displacement Sensing Based on Single-Walled Carbon Nanotubes. *Nano Lett.* **2006**, *6*, 1449–1453.
19. Bunch, J. S.; van der Zande, A. M.; Verbridge, S. S.; Frank, I. W.; Tanenbaum, D. M.; Parpia, J. M.; Craighead, H. G.; McEuen, P. L. Electromechanical Resonators from Graphene Sheets. *Science* **2007**, *315*, 490–493.
20. Nagapriya, K. S.; Berber, S.; Cohen-Karni, T.; Segev, L.; Srur-Lavi, O.; Tománek, D.; Joselevich, E. Origin of Torsion-Induced Conductance Oscillations in Carbon Nanotubes. *Phys. Rev. B* **2008**, *78*, 165417-1–165417-5.
21. Poot, M.; van der Zant, H. S. J. Nanomechanical Properties of Few-Layer Graphene Membranes. *Appl. Phys. Lett.* **2008**, *92*, 063111-1–063111-3.
22. Sun, L.; Li, Q.; Ren, H.; Su, H.; and Shi, Q. W.; Yang, J. Strain Effect on Electronic Structures of Graphene Nanoribbons: A First-Principles Study. *J. Chem. Phys.* **2008**, *129*, 074704-1–074704-6.
23. Hod, O.; Scuseria, G. E. Electromechanical Properties of Suspended Graphene Nanoribbons. *Nano Lett.* **2009**, *9*, 2619–2622.
24. Pantano, A.; Nardelli, M. B. Simulation of the Electromechanical Behavior of Multiwall Carbon Nanotubes. *ACS Nano* **2009**, *3*, 3266–3272.
25. Xu, Z.; Buehler, M. J. Strain Controlled Thermomutability of Single-Walled Carbon Nanotubes. *Nanotechnology* **2009**, *20*, 185701-1–185701-6.
26. Marom, N.; Bernstein, J.; Garel, J.; Tkatchenko, A.; Joselevich, E.; Kronik, L.; Hod, O. Stacking and Registry Effects in Layered Materials: The Case of Hexagonal Boron Nitride. *Phys. Rev. Lett.* **2010**, *105*, 046801-1–046801-4.
27. Chopra, N. G.; Benedict, L. X.; Crespi, V. H.; Cohen, M. L.; Louie, S. G.; Zettl, A. Fully Collapsed Carbon Nanotubes. *Nature* **1995**, *377*, 135–138.
28. Giusca, C. E.; Tison, Y.; Silva, S. R. P. Evidence for Metal-Semiconductor Transitions in Twisted and Collapsed Double-Walled Carbon Nanotubes by Scanning Tunneling Microscopy. *Nano Lett.* **2008**, *8*, 3350–3356.
29. Zhang, D.-B.; James, R. D.; Dumitrică, T. Dislocation Onset and Nearly-Axial Glide in Carbon Nanotubes under Torsion. *J. Chem. Phys.* **2009**, *130*, 071101−1−071101−4.
30. Vercosa, D. G.; Barros, E. B.; Souza Filho, A. G.; Mendes Filho, J.; Samsonidze, G. G.; Saito, R.; Dresselhaus, M. S. Torsional Instability of Chiral Carbon Nanotubes. *Phys. Rev. B* **2010**, *81*, 165430−1165430−5.
31. Zhang, D.-B.; Dumitrică, T.; Seifert, G. Helical Nanotube Structures of MoS_2 with Intrinsic Twisting: An Objective Molecular Dynamics Study. *Phys. Rev. Lett.* **2010**, *104*, 065502-1–065502-4.
32. Zhang, D.-B.; Dumitrică, T. Elasticity of Ideal Single-Walled Carbon Nanotubes *via* Symmetry-Adapted Tight-Binding

Objective Modeling. *Appl. Phys. Lett.* **2008**, *93*, 031919-1–031919-3.
33. Saito, R.; Dresselhaus, G.; Dresselhaus, M. S. *Physical Properties of Carbon Nanotubes*; Imperial College Press: London, 1998.
34. Damnjanović, M.; Milošević, I.; Vuković, T.; Sredanović, R. Full Symmetry, Optical Activity, and Potentials of Single-Wall and Multiwall Nanotubes. *Phys. Rev. B* **1999**, *60*, 2728–2739.
35. Zhang, D.-B.; James, R. D.; Dumitrică, T. Electromechanical Characterization of Carbon Nanotubes in Torsion *via* Symmetry-Adapted Tight-Binding Objective Molecular Dynamics. *Phys. Rev. B* **2009**, *80*, 115418-1–115418-5.
36. Dumitrică, T.; James, R. D. Objective Molecular Dynamics. *J. Mech. Phys. Solids* **2007**, *55*, 2206–2236.
37. Zhang, D.-B.; Hua, M; Dumitrică, T. Stability of Polycrystalline and Wurtzite Si Nanowires *via* Symmetry-Adapted Tight-Binding Objective Molecular Dynamics. *J. Chem. Phys.* **2008**, *128*, 084104-1–084104-9.
38. White, C. T.; Robertson, D. H.; Mintmire, J. W. Helical and Rotational Symmetries of Nanoscale Graphitic Tubules. *Phys. Rev. B* **1993**, *47*, 5485–5488(R).
39. Allen, P. B. Nanocrystalline Nanowires: III. Electrons. *Nano Lett.* **2007**, *7*, 1220–1223.
40. Porezag, D.; Frauenheim, Th.; Köhler, Th.; Seifert, G.; Kaschner, R. Construction of Tight-Binding-like Potentials on the Basis of Density-Functional Theory: Application to Carbon. *Phys. Rev. B* **1995**, *51*, 12947–12957.
41. Carlson, A; Dumitrică, T. Extended Tight-Binding Potential for Modelling Intertube Interactions in Carbon Nanotubes. *Nanotechnology* **2007**, *18*, 065706-1–065706-5.
42. Elliott, J. A.; Sandler, J. K. W.; Windle, A. H.; Young, R. J.; Shaffer, M. S. P. Collapse of Single-Wall Carbon Nanotubes is Diameter Dependent. *Phys. Rev. Lett.* **2004**, *92*, 095501-1–095501-4.
43. More precisely, γ is the average over the coupling region of the interlayer hopping element γ_1 of graphite. See Malard, L. M.; et al. Probing the Electronic Structure of Bilayer Graphene by Raman Scattering. *Phys. Rev. B* **2007**, *76*, 201401-1–201401-5(R).
44. The shear strain on a C−C bond is the ratio between its circumferential displacement and its axial projection.
45. Nikiforov, I.; Zhang, D.-B.; James, R. D.; Dumitrică, T. Wavelike Rippling in Multiwalled Carbon Nanotubes under Pure Bending. *Appl. Phys. Lett.* **2010**, *96*, 123107-1–123107-3.
46. James, R. D. Objective Structures. *J. Mech. Phys. Solids* **2006**, *54*, 2354–2390.
47. Qin, L.-C.; Iijima, S. Twisting of Single-Walled Carbon Nanotube Bundles. *Mater. Res. Soc. Symp. Proc.* **2000**, *593*, 33–36.
48. Qian, D.; Liu, W. K.; Ruoff, R. S. Load Transfer Mechanism in Carbon Nanotube Ropes. *Compos. Sci. Technol.* **2003**, *63*, 1561–1569.
49. Delaney, P.; Joon Choi, H.; Ihm, J.; Louie, S. G.; Cohen, M. L. Broken Symmetry and Pseudogaps in Ropes of Carbon Nanotubes. *Nature* **1998**, *391*, 466–468.
50. Shenoy, V. B.; Reddy, C. D.; Ramasubramaniam, A.; Zhang, Y. W. Edge-Stress-Induced Warping of Graphene Sheets and Nanoribbons. *Phys. Rev. Lett.* **2008**, *101*, 245501-1–245501-4.
51. Bets, K. V.; Yakobson, B. I Spontaneous Twist and Intrinsic Instabilities of Pristine Graphene Nanoribbons. *Nano Res.* **2009**, *2*, 161–166.
52. Rurali, R.; Hernandez, E. Trocadero: A Multiple-Algorithm Multiple-Model Atomistic Simulation Program. *Comput. Mater. Sci.* **2003**, *28*, 85–106.